Journal of Solid State Chemistry 182 (2009) 196–202

Contents lists available at ScienceDirect

Journal of Solid State Chemistry

journal homepage: www.elsevier.com/locate/jssc

Low-dimensional compounds containing cyano groups. XVII. Crystal structure, spectroscopic, thermal and magnetic properties of $[Cu(bmen)_2][Pt(CN)_4]$ (*bmen* = *N*,*N*′-dimethylethylenediamine)

Ivan Potočňák [a,*], Martin Vavra [a], Erik Čižmár [b,c], Marcela Kajňaková [b], Alena Radváková [b], Dirk Steinborn [d], Sergei A. Zvyagin [c], Jochen Wosnitza [c], Alexander Feher [b]

[a] Department of Inorganic Chemistry, Institute of Chemistry, P.J. Šafárik University, Moyzesova 11, SK-04154 Košice, Slovakia
[b] Centre of Low Temperature Physics of the Faculty of Science of P.J. Šafárik University and IEP SAS, Park Angelinum 9, SK-04154 Košice, Slovakia
[c] Dresden High Magnetic Field Laboratory (HLD), Forschungszentrum Dresden-Rossendorf, D-01314 Dresden, Germany
[d] Institute of Inorganic Chemistry, Martin-Luther-University, Halle-Wittenberg, Kurt-Mothes-Str. 2, D-06120 Halle, Germany

ARTICLE INFO

Article history:
Received 23 June 2008
Received in revised form
1 October 2008
Accepted 12 October 2008
Available online 25 October 2008

Keywords:
1D crystal structure
$[Pt(CN)_4]^{2-}$ anion
Hydrogen bonds
Thermal studies
Spectroscopic studies
Heisenberg square lattice

ABSTRACT

The synthesis, structural analysis, spectroscopic studies, susceptibility and specific-heat measurements of $\{[Cu(bmen)_2][Pt(CN)_4]\}_n$ (*bmen* = *N*,*N*′-dimethylethylenediamine) are presented. X-ray crystal-structure analysis revealed that the $[Pt(CN)_4]^{2-}$ building blocks are combined with $[Cu(bmen)_2]^{2+}$ units to form a chain-like structure along the *a* axis. The Cu(II) atoms are hexacoordinated by four nitrogen atoms in the equatorial plane belonging to two molecules of bidentate *bmen* ligands with average Cu–N distance of 2.043(18) Å. The axial positions are occupied by two nitrogen atoms from bridging $[Pt(CN)_4]^{2-}$ anions at a longer axial Cu–N distance of 2.490(4) Å. The compound is characterized by the presence of a weak antiferromagnetic exchange coupling $J/k_B = 0.6$ K. Despite the one-dimensional (1D) character of the structure, the analysis of the magnetic properties and specific heat at very low temperatures shows that $[Cu(bmen)_2][Pt(CN)_4]$ behaves as a two-dimensional (2D) square-lattice Heisenberg magnet with weak interlayer coupling.

1. Introduction

The field of transition metal cyanide chemistry has a remarkable history that spans almost three centuries, dating back to the earlier eighteenth century. The wide availability of cyano complexes together with their diverse bonding and structural chemistry has led to their widespread applications in the field of materials chemistry [1]. Several detailed reviews on metal cyanides describing their structures, reactivity and physical properties have been published over the years [2–4]. A review on the coordination modes of the $[Pt(CN)_4]^{2-}$ anion has been presented in our previous paper [5].

The ability of the cyano group to link various metal ions leads to a wide diversity of structural architectures ranging from discrete oligonuclear complexes to various more-dimensional networks. Recently, cyano complexes with various degrees of structural dimensionality have often been the subject of magnetic studies. In this case, the cyano group or cyano complex anion (with a diamagnetic central atom), in addition to its structural function, also exhibits an important electronic function: it forms an exchange path mediating the interaction among spins localized on paramagnetic centers. The dimensionality of the magnetic subsystem is fundamental for cooperative processes, but it does not mean that the magnetic and structural dimensionality must be the same. The increase of magnetic dimensionality can be caused by the influence of hydrogen bonds (HBs), π–π and also dipole–dipole interactions [6,7].

Previous studies of $[Cu(L)_2][M(CN)_4]$ (M = Ni, Pd and Pt; L is ethylenediamine = *en*; *N*-methylethylenediamine = *men*; asymmetric *N*,*N*-dimethylethylenediamine = *dmen*; symmetric *N*,*N*′-dimethylethylenediamine = *bmen*) revealed that despite the 1D character of their structure they behave as 2D Heisenberg antiferromagnets (HAF) [5,8–11]. The 2D character of the magnetic subsystem can be explained by the formation of HBs linking the neighboring chains and thus serving as exchange paths for magnetic interactions. In the isotropic case of the 2D HAF model, thermal fluctuations destroy magnetic long-range order at any finite temperature as known from the Mermin–Wagner theorem [12]. However, the presence of even very low uniaxial anisotropy of Ising type, induces a finite-temperature phase transition into the Néel ordered state [13]. An anisotropy of the *XY* type leads to a Berezinski–Kosterlitz–Thouless (BKT) transition

* Corresponding author. Fax: +421 55 62 221 24.
E-mail address: ivan.potocnak@upjs.sk (I. Potočňák).

0022-4596/$ - see front matter © 2008 Elsevier Inc. All rights reserved.
doi:10.1016/j.jssc.2008.10.017

[14–17] at finite temperature T_{BKT}. Nevertheless, it is very difficult to observe a BKT transition in real magnets due to the presence of interlayer coupling, which induces a second-order phase transition into a state with 3D magnetic order. In this paper, we present the results of infrared and UV–VIS spectroscopy, thermal and X-ray crystal-structure analyses, electron spin resonance, magnetic and specific-heat measurements of the new complex $[Cu(bmen)_2][Pt(CN)_4]$ (**1**), which was synthesized with the aim to tune the ratio of interlayer and intralayer exchange couplings by suppressing some of the HBs in comparison to materials studied in our previous work [5].

2. Experimental

2.1. Materials

Copper chloride dihydrate ($CuCl_2 \cdot 2H_2O$) and *bmen* ($C_4H_{12}N_2$) were of Merck quality and used as received. $K_2[Pt(CN)_4] \cdot 3H_2O$ was prepared according to the literature [18] using $H_2[PtCl_6] \cdot 6H_2O$ from Chempur as starting platinum-containing material.

2.2. Synthesis

Into stirring 10 ml water–methanol solution, (1:1) of $CuCl_2$ (0.5 mmol; 0.085 g of $CuCl_2 \cdot 2H_2O$), *bmen* (2 mmol; 0.22 ml of *bmen*) was added and finally 10 ml aqueous solution of $K_2[Pt(CN)_4]$ (0.5 mmol; 0.216 g of $K_2[Pt(CN)_4] \cdot 3H_2O$) was added after 30 min. As a result a blue precipitate was immediately formed. This precipitate was dissolved by the addition of 20 ml of concentrated ammonia solution to the reaction mixture. After 3 days, blue crystals of **1** were filtered off and dried on air. Yield—86%. Anal. Calc. for $C_{12}H_{24}N_8CuPt$—C: 26.74; H: 4.49; N: 20.78. Found—C: 26.44; H: 4.96; N: 20.43%.

2.3. Physical measurements

Elemental analysis for C, H and N was carried out using an LECO CHNS-932. The IR spectrum was recorded on an Avatar 330 FT-IR Spectrometer from ThermoNicolet by the method of KBr pellets in the range from 4000 to 400 cm^{-1}. Reflectance UV–VIS spectrum was measured with Perkin–Elmer UV/VIS/NIR Spectrometer Lambda 19 in the range from 200 to 1100 nm. The thermal investigation was performed using NETZSCH STA 409 PC/PG thermal analyzer under dynamic conditions in nitrogen atmosphere with a heating rate of 6 °C/min to 700 °C using 30.094 mg of the sample and Al_2O_3 crucibles. ESR data were collected at low temperatures in an X-band Bruker ELEXSYS E500 spectrometer. Measurements of the magnetic susceptibility have been carried out using a commercial SQUID magnetometer in the temperature range from 2 to 300 K. The background contribution from the gelatine capsule to the magnetic moment of the sample has been subtracted. The specific heat of $[Cu(bmen)_2][Pt(CN)_4]$ was studied in the temperature range from 125 mK to 3 K in zero magnetic field using a dual-slope technique [19] in a dilution refrigerator made by Oxford Instruments (model TLE 2000). For monitoring the temperature of the sample a RuO_2 resistor of Dale type with a nominal value of 1 kΩ calibrated against a commercial Lake Shore thermometer GR200A-30 was used. The experimental inaccuracy of the specific-heat measurements is less then 4%. The ESR and magnetic measurements have been carried out on powdered samples, while for the thermodynamic experiments pelletized powder samples have been used.

Table 1
Crystal data and structure refinement of **1**.

Empirical formula	$C_{12}H_{24}N_8CuPt$
Formula weight	539.01
Temperature	293(2) K
Wavelength	0.71073 Å
Crystal system	Orthorhombic
Space group	*Pbca*
Unit cell dimensions	10.2938(4) Å 12.5923(5) Å 13.5164(5) Å
Volume	1752.03(12) $Å^3$
Z; density (calculated)	4; 2.043 g cm^{-3}
Absorption coefficient	9.198 mm^{-1}
F(000)	1036
Crystal shape, color	Needle, blue
Crystal size	0.43 × 0.15 × 0.11 mm
θ range for data collection	2.97°–25.50°
Index ranges	$-12 \leqslant h \leqslant 11$, $-6 \leqslant k \leqslant 15$, $-16 \leqslant l \leqslant 16$
Absorption correction	Analytical
Max. and min. transmission	0.396 and 0.214
Reflections collected/unique	5131/1638 [R(int) = 0.0166]
Refinement method	Full-matrix least-squares on F^2
Data/restraints/parameters	1638/0/105
Goodness-of-fit on F^2	0.982
Final R factors [$I > 2\sigma(I)$]	$R_1 = 0.0151$, $wR_2 = 0.0381$
R factors (all data)	$R_1 = 0.0527$, $wR_2 = 0.0430$
Hydrogen atoms	Constrained
Weighting scheme	$w = 1/[\sigma^2(F_o^2)+(0.0180P)^2]$ where $P = (F_o^2+2F_c^2)/3$
Largest diff. peak and hole	0.290 and −0.488 e$Å^{-3}$

2.4. X-ray data collection and structure refinement

A summary of crystal data and structure refinement for **1** is presented in Table 1. The crystal structure of **1** was determined using an Oxford Diffraction Xcalibur2 diffractometer equipped with a Sapphire2 CCD detector. Crysalis CCD [20] was used for data collection while Crysalis RED [20] was used for the cell refinement, data reduction and absorption correction. The structure was solved by the direct method with SHELXS97 [21] and subsequent Fourier syntheses using SHELXL97 [21]. The anisotropic displacement parameters were refined for all non-H atoms. The H atoms were placed in calculated positions and refined riding on their parent C or N atoms with C–H distances of 0.97 and 0.96 Å for methylene and methyl H atoms, respectively, and with N–H distances of 0.91 Å for amino H atoms, and $U_{iso}(H) = 1.2U_{eq}$ (C or N). A geometric analysis was performed using SHELXL97 and PARST [22]. DIAMOND [23] was used for molecular graphics.

3. Results and discussion

3.1. Infrared spectroscopy

Several significant bands appear in the IR spectrum of **1** (Table 2), including the ν(N–H), ν(C–H), $\nu(C\equiv N)$, $\delta(-CH_3)$, $\omega(-CH_2-)$, $\tau(-CH_2-)$, $\tau(-CH_3)$, τ(–NHR), ν(C–N), ν(C–C), $\sigma(-CH_2-)$ and ν(Pt–C) vibrations which confirm the presence of *bmen* and the $[Pt(CN)_4]^{2-}$ anion. Individual bands were assigned according to [24,25]. Special attention is paid to the $\nu(C\equiv N)$ stretching vibrations which prove the presence of $[Pt(CN)_4]^{2-}$ in the prepared compound and whose positions are an important tool to distinguish between terminal and bridging character of cyano groups. This position is observed at 2080 cm^{-1} in ionic KCN as a single absorption band [25]. Upon coordination to a metal, the $\nu(C\equiv N)$ mode shifts to higher frequencies and the range of $\nu(C\equiv N)$ for cyanoplatinates(II) with terminal cyano ligands

Table 2
IR spectrum of **1** (cm^{-1}).

ν(N–H)	3301 vs
	3206 vs
ν(C–H)	3014 w
	2967 m
	2940 s
	2884 m
ν(C≡N)	2132 s
	2122 vs
δ(–CH_3)	1481 s
	1467 m
	1453 s
	1435 m
	1424 sh
ω(–CH_2–)	1372 m
τ(–CH_2–)	1279 m
τ(–CH_3)	1148 m
τ(–NHR)	1084 s
ν(C–N)	1036 s
	1024 s
ν(C–C)	966 vs
σ(–CH_2–)	861 m
	827 w
ν(Pt–C)	499 m
	451 w
	397 m

ν—stretching, δ—scissoring, ω—wagging, τ—twisting, σ—rocking vibrations, vs—very strong, s—strong, m—middle, w—weak vibrations, sh—shoulder.

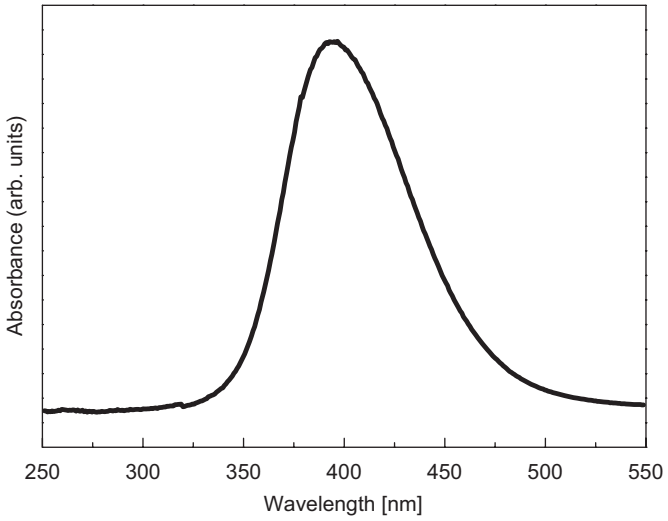

Fig. 1. Reflectance UV–VIS spectrum of **1**.

extends from 2120 to 2140 cm^{-1} [26]. Generally, if the M–C≡N group of an $[M(CN)_4]^{2-}$ anion forms an M–C≡N–M'-type bridge, the ν(C≡N) band shifts to even higher frequency [25], and a single ν(C≡N) band can be split into two bands due to the presence of the terminal and bridging cyano groups in the complex [27,28]. According to this, the bands recorded at 2122 and 2132 cm^{-1} in **1**, can be assigned to ν(C≡N) stretching vibrations of terminal and bridging cyano groups, respectively. The intensity of both bands is almost the same, in agreement with the same number of terminal and bridging cyano groups in the structure of **1**. Two ν(C≡N) vibrations have also been observed in other $[Cu(bmen)_2][M(CN)_4]$ (M = Ni and Pd) [10,11]) compounds. On the other hand, in the spectra of $[Cu(en)_2][Pt(CN)_4]$ [5] and $[Cu(dmen)_2][M(CN)_4]$ compounds (M = Ni, Pd and Pt) [5,10,29] only one ν(C≡N) absorption band has been observed. The discrepancy in the number of observed vibrations may be explained by the different local symmetry of $[Pt(CN)_4]^{2-}$ anions in the discussed compounds, whereas the C≡N bonds in $[Cu(en)_2][Pt(CN)_4]$ and $[Cu(dmen)_2][M(CN)_4]$ compounds differ only by 0.002 Å, corresponding difference in **1** is 0.016 Å. Thus, the local symmetry of $[Pt(CN)_4]^{2-}$ anions in $[Cu(en)_2][Pt(CN)_4]$ and $[Cu(dmen)_2][M(CN)_4]$ compounds is D_{4h} with only one E_u IR active vibration and the local symmetry of $[Pt(CN)_4]^{2-}$ anion in **1** is D_{2h} with B_{2u} and B_{3u} IR active vibrations. The different local symmetry is also reflected by the different Cu–N(cyano) bond lengths in **1** and $[Cu(bmen)_2][M(CN)_4]$ compounds on the one hand, and $[Cu(en)_2][Pt(CN)_4]$ and $[Cu(dmen)_2][M(CN)_4]$ compounds on the other hand. The corresponding Cu–N(cyano) bond length in **1** is 2.490(4) Å and analogous distances in other $[Cu(bmen)_2][M(CN)_4]$ compounds are only a little shorter. However, these distances in the $[Cu(en)_2][Pt(CN)_4]$ and $[Cu(dmen)_2][M(CN)_4]$ compounds are within the range of 2.537(1)–2.600(5) Å and, therefore, the bridging cyano groups adopt partially ionic character and their behavior is rather close to the terminal one. In accordance, the wavenumbers of the corresponding vibrations decrease and eventually may be overlapped by the vibrations of terminal cyano groups. Therefore, only one ν(C≡N) absorption band in their IR spectra has been observed.

3.2. UV–VIS spectroscopy

The reflectance UV–VIS spectrum of **1** (Fig. 1) was taken as described earlier. A broad almost symmetric band with a maximum at 397 nm is observed in the spectrum. This could be assigned to the $^2B_{1g} \rightarrow {}^2E_g$ transition suggesting a deformed octahedral coordination of the CuN_6 chromophoric group.

3.3. Thermal studies

The usual way of thermal decomposition of cyano complexes is characterized by liberation of *N*-donor ligands followed by separated decomposition of all cyano groups in one step. In accordance with this and with the results of thermal decompositions of previously studied similar compounds [5], the thermal decomposition of **1** is a multistage process. The compound **1** is stable up to 202 °C. In the temperature range 202–300 °C, a weight loss of 17.0% corresponding to the release of one *bmen* molecule (calc. 16.4%) is observed during the overlapping of slightly endothermic and exothermic stages as evidenced by a minimum and a maximum in the differential thermal analysis (DTA) at 233 and 248 °C, respectively. Within 300–488 °C the decomposition continues with liberating the second *bmen* molecule, reflected as very small endothermic effect followed by a slight exothermic process (minimum and maximum in DTA at 350 and 460 °C, respectively). The release of the second *bmen* molecule is overlapping with a strongly exothermic decomposition of the cyanides completed at 670 °C. The total weight loss of these stages is 29.0% that corresponds to the decomposition of one *bmen* molecule and, contrary to the previous decompositions of similar compounds, only three of four cyano groups (calc. 14.5%). Their decomposition includes the oxidation of cyano groups to form one and a half cyanogen molecules during the reduction of one Pt(II) to a Pt atom and one Cu(II) to a Cu(I) atom. The final thermal decomposition product is a mixture of CuCN and metallic Pt (solid residue 54.0%; calculated 52.8%). The most probable thermal decomposition

scheme for **1** could be given as:

$$[Cu(bmen)_2][Pt(CN)_4] \xrightarrow[-bmen]{202-300\,^{\circ}C} [Cu(bmen)Pt(CN)_4] \xrightarrow[-bmen]{300-488\,^{\circ}C} CuPt(CN)_4$$

$$CuPt(CN)_4 \xrightarrow[-1.5(CN)_2]{488-670\,^{\circ}C} CuCN + Pt$$

3.4. X-ray crystallography

X-ray analysis has revealed that the crystal structure of **1** consists of 1D zigzag chains running along the [100] direction. An ORTEP view of this compound is depicted in Fig. 2 with the atomic numbering scheme; selected bond lengths and bond angles of **1** are given in Table 3. The structure of **1** is similar to the structures of compounds with the general formula $[Cu(L)_2][M(CN)_4]$ mentioned above. In **1**, both Cu(II) and Pt(II) ions sit on inversion centers. The Cu(II) ion has a six-fold coordination, consisting of the four nitrogen atoms of two *bmen* ligands in the equatorial plane and two nitrogen atoms from different bridging cyano groups in the axial positions. The Cu–N bond distances in the equatorial plane have an average value of 2.043(18) Å, while weak axial interactions, characteristic of d^9 systems, give rise to a Cu–N(cyano) bond length of 2.490(4) Å. Cu–N(amine) bond lengths are in comparison with other $[Cu(L)_2][Pt(CN)_4]$ compounds either equal (L = *en*) or different (L = *dmen*) [5].

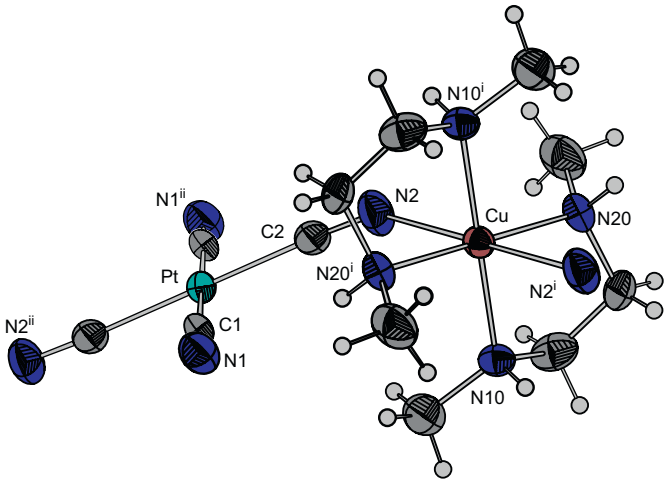

Fig. 2. Structure of **1**. Displacement ellipsoids are plotted at the 50% probability level and H atoms are shown as small spheres of arbitrary radii. (Symmetry codes: (i) 1−*x*, −*y*, −*z*; (ii) −*x*, −*y*, −*z*.)

Table 3
Selected bond lengths (Å) and bond angles (°) of **1**.

Cu–N2	2.490 (4)
Cu–N10	2.056 (4)
Cu–N20	2.030 (4)
Pt–C1	1.995 (5)
Pt–C2	1.993 (5)
C1–N1	1.122 (5)
C2–N2	1.138 (5)
C1–Pt–C2	89.19 (17)
Cu–N2–C2	135.6 (4)
N1–C1–Pt	178.6 (4)
N2–C2–Pt	175.1 (4)
N20–Cu–N10	84.63 (15)
N20–Cu–N2	94.40 (13)
N10–Cu–N2	90.83 (13)

The Cu–N2 bonds in the axial positions are slightly tilted from the normal to the CuN_4 plane (the tilt angle between the apical axis and the normal to the plane is 4.40°), forming a slightly distorted and tetragonally elongated octahedral geometry.

The geometry of the $[Pt(CN)_4]^{2-}$ anion is square planar, with C1–Pt–C2 bond angle of 90.81(17). The Pt–C and C≡N bond distances (Table 3) are in an expected range, with regard to both bridging and terminal modes, with only small differences to the other structures [5,30]. The Pt–C≡N bond angles are almost linear what is also in a very good agreement with other compounds [5,30].

The structure of **1** is stabilized by a pair of weak HBs shown in Fig. 3. One of them, the interchain HB N10–H10···N1, with an N10···N1 length of 3.117(5) Å (Table 4), connects the chains into 2D sheets in the *ab* plane; a similar situation was observed in the structure of $[Cu(dmen)_2][Pt(CN)_4]$ too, which contains an asymmetric *N*,*N*-dimethylethylenediamine. In comparison to that structure, the N20···N1 distance of 3.247(5) Å (Table 4) indicates an N20–H20···N1 intrachain HB interaction in **1** which was not observed in the structure containing *dmen*. We can conclude that due to the presence of one hydrogen atom on each nitrogen donor atom of *bmen* there is one additional intrachain HB interaction. Nevertheless, the HB system in **1** is strongly reduced in comparison to the similar compound with *en* [5].

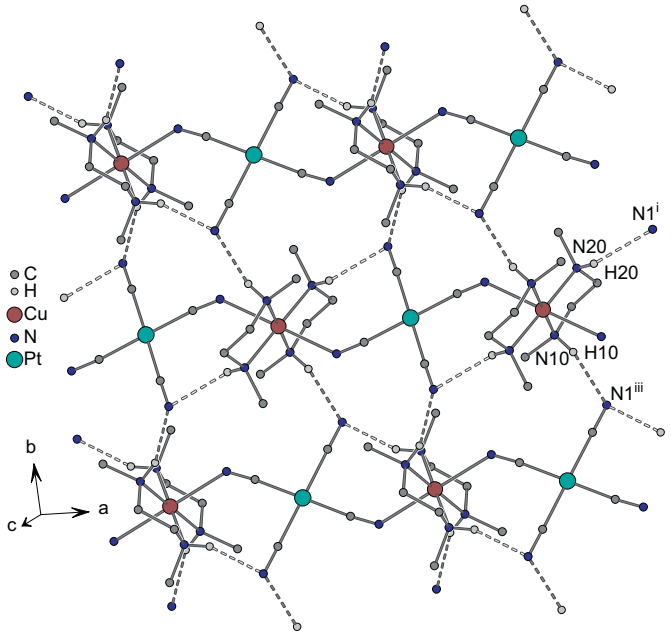

Fig. 3. HB system in **1** viewed along the chain direction. The interchain HBs connecting chains into sheets are represented by black dashed lines, while intrachain HBs are represented by empty dashed lines. Only hydrogen atoms of amino groups are shown for clarity. (Symmetry codes: (i) 1−*x*, −*y*, −*z*; (iii) 1/2+*x*, −1/2−*y*, −*z*.)

Table 4
Hydrogen bonds for **1** [Å and °].

D–H···A	D–H	H···A	D···A	D–H···A
N20–H20···N1^{i}	0.91	2.48	3.247 (5)	142.7
N10–H10···N1^{iii}	0.91	2.26	3.117 (5)	157.3

Symmetry transformations used to generate equivalent atoms: (i) 1−*x*, −*y*, −*z*; (iii) 1/2+*x*, −1/2−*y*, −*z*.

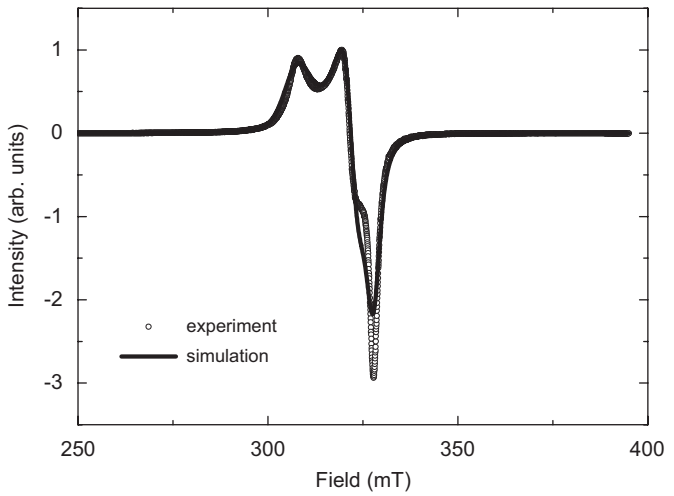

Fig. 4. Comparison of the experimental ESR spectrum of [Cu(*bmen*)$_2$][Pt(CN)$_4$] measured at 9.4 GHz and the EasySpin [31] simulation for $g_x = 2.05 \pm 0.005$, $g_y = 2.09 \pm 0.005$, $g_z = 2.18 \pm 0.005$ and $\Delta B = 3.5 \pm 0.2$ mT including the anisotropic broadening parameters $\Delta B_x = 1.8 \pm 0.2$ mT, $\Delta B_y = 2.8 \pm 0.2$ mT and $\Delta B_z = 6.8 \pm 0.2$ mT due to unresolved hyperfine coupling.

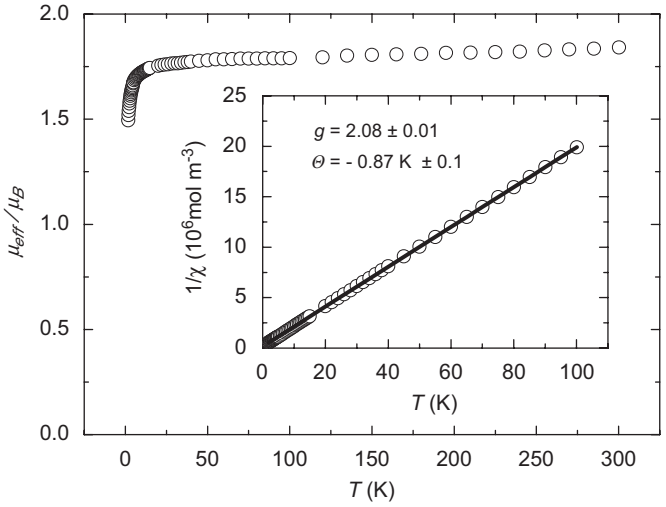

Fig. 5. Effective magnetic moment of [Cu(*bmen*)$_2$][Pt(CN)$_4$]. The inset shows the temperature dependence of the inverse susceptibility (circles) with a fit to the Curie–Weiss law (solid line).

3.5. Magnetic properties

The ESR spectra of **1** obtained at 2 K on powdered samples (Fig. 4) have been analyzed using the ESR spectra simulation package EasySpin [31]. The best fit to the experimental data using a least-squares method (Fig. 4) has been obtained for the following set of parameters: $g_x = 2.05 \pm 0.005$, $g_y = 2.09 \pm 0.005$, $g_z = 2.18 \pm 0.005$ and simple isotropic linewidth $\Delta B = 3.5 \pm 0.2$ mT. The hyperfine structure expected for Cu(II) atoms could not be resolved in the spectrum suggesting the existence of exchange couplings between magnetic centers [32], but its influence is taken into account using the anisotropic broadening parameters $\Delta B_x = 1.8 \pm 0.2$ mT, $\Delta B_y = 2.8 \pm 0.2$ mT and $\Delta B_z = 6.8 \pm 0.2$ mT. The anisotropic g-factors are consistent with the axial type of anisotropy due to the Jahn–Teller effect typical for spin $S = 1/2$ Cu(II) ions including the influence of a weak rhombic distortion of the coordination octahedron. The deviations between the fit and data might be attributed to the low-dimensional character of the magnetic subsystem. The results confirm that the electronic ground state of the Cu(II) ion is described by a wave function of d_{z^2} symmetry and the exchange paths will propagate along the directions determined by the lobes of the $d_{x^2-y^2}$ orbital.

The magnetic susceptibility of a powdered sample measured at 0.1 T was corrected for the diamagnetic contribution of the material which was estimated using Pascal's constants [33] to be $\chi_{DIA} = -2.9586 \times 10^{-9}$ m^3 mol^{-1}. From the susceptibility at $T = 300$ K, the effective magnetic moment may be quantified and yields a value typical for a Cu(II) cation with d^9 configuration, namely $\mu_{eff}/\mu_B = 1.85$ (see Fig. 5). No difference between the susceptibility of the zero-field cooled and field-cooled sample has been observed down to 2 K, which suggests that no long-range order appears above 2 K. The temperature dependence of the susceptibility is characterized by a Curie-like behavior without the short-range-order maximum expected at low temperatures for the low-dimensional system with antiferromagnetic exchange coupling. Consequently, only an estimate of the effective strength of the exchange coupling zJ/k_B, where z is the number of the nearest neighbors, by fitting the Curie–Weiss law to the experimental data in the temperature range 2–100 K is obtained. The fit yields the values $zJ/k_B = -3.48 \pm 0.05$ K and $g = 2.08 \pm 0.01$ (inset in Fig. 5).

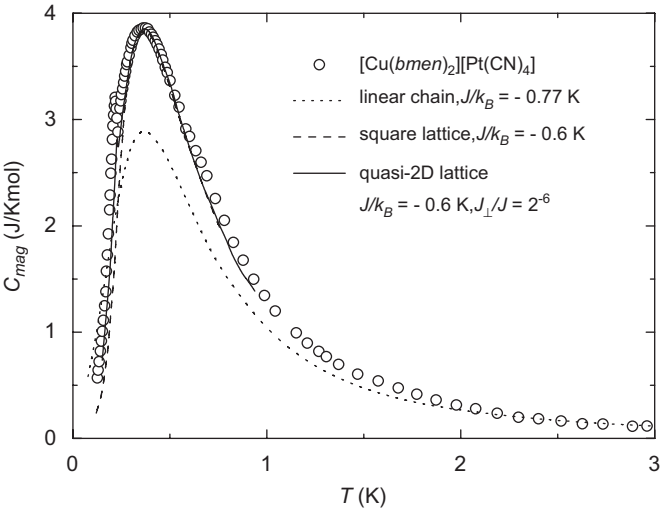

Fig. 6. Magnetic specific heat of [Cu(*bmen*)$_2$][Pt(CN)$_4$] compared to the HAF linear-chain model with $J/k_B = -0.77$ K (dotted line), while the dashed line represents the HAF square-lattice model with $J/k_B = -0.6$ K. The solid line represents the quasi-2D HAF model with intralayer exchange interaction $J/k_B = -0.6$ K and an interlayer exchange interaction given by $J_\perp/J = 2^{-6} \cong 0.0156$.

The specific heat of **1** has been investigated in zero magnetic field in the temperature range 125 mK–3 K with the aim to clarify the magnetic structure and dimensionality of the systems. Since the compound is a magnetic insulator, only the lattice contribution to the total specific heat was subtracted after fitting the high-temperature region to the equation $C = aT^{-2} + bT^3$, where aT^{-2} describes the high-temperature expansion of the magnetic specific heat, while bT^3 represents the low-temperature description of the lattice contribution in the Debye approximation. The best fit was obtained for $a = 1.101$ J Kmol^{-1} and $b = 0.0211$ J K^{-4} mol^{-1}. The temperature dependence of the magnetic specific heat displays a round maximum at $T_{max} = 0.37$ K and a λ-like anomaly, associated with long-range ordering, at $T_\lambda = 0.22$ K (Fig. 6). After subtraction of the lattice contribution, the magnetic entropy has been calculated from the experimental data with simple extrapolations used for $T \to 0$ and $T \to \infty$. The calculated magnetic entropy reaches the theoretically predicted value $S_{theor} = R$

$\ln(2S+1) = 5.76\,J\,K^{-1}\,mol^{-1}$ for magnetic systems with spin $S = 1/2$. The magnetic entropy removed above T_λ represents 86% of the total magnetic entropy suggesting a low-dimensional character of the studied systems.

Considering the topology of covalent and possible HBs, the magnetic specific heat of $[Cu(bmen)_2][Pt(CN)_4]$ has been compared to the theoretical models for a HAF linear-chain [34], an isotropic HAF square-lattice [35,36] and quasi-2D HAF square-lattice magnet [37] (Fig. 6). The exchange coupling parameters obtained from the comparison are $J/k_B = -0.77$ and -0.6 K for the HAF linear-chain model and the HAF square-lattice model, respectively. Despite the chain-like crystal structure of the title compound better agreement is obtained for the HAF square lattice models, suggesting the dominant role of HBs mediating the exchange interaction in the directions of the magnetic $d_{x^2-y^2}$ orbitals oriented within the equatorial plane of the local octahedron of the Cu(II) atoms. The values of the exchange couplings are in good agreement with the estimate of the effective strength of the exchange coupling from the Curie constant.

As mentioned above, no magnetic long-range order at any finite temperature should be observed for an isotropic 2D HAF model [12] and the origin of the λ-like anomaly should be discussed. First, we estimate the value of a possible exchange anisotropy $\Delta/J = ((g_\parallel - g_\perp)/g)^2 = 0.0027$, where $J\perp = (1+\Delta)J$, induced by the anisotropy of the g-factor [38]. Even such a weak easy-axis exchange anisotropy leads to a 2D long-range order of Ising type [13]. Nevertheless, the estimated value of the exchange coupling $J/k_B = -0.6$ K for the square-lattice model is about 2/3 of the expected value for a 2D Ising transition to appear at 0.22 K [13]. In addition, the effect of a very weak interlayer interaction in a 2D HAF is to induce a transition to a 3D long-range ordered state at finite temperature with a tiny λ-like anomaly as shown in the work of Sengupta [37]. The height of the maximum at $T_{max} = 0.37$ K and the position of the λ-like anomaly at $T_\lambda = 0.22$ K suggests the influence of an interlayer coupling with a strength less then $J_\perp = 10$ mK ($J_\perp/J = 2^{-6}$). In the range $0.001 \leqslant J_\perp/J \leqslant 1$ we can estimate the interlayer coupling from the critical temperature using the formula $T_\lambda = 4\pi\rho S/[2.43 - \ln(J_\perp/J)]$, where $\rho_S = 0.183J$ is the spin stiffness [39], resulting in $J_\perp = 6.5$ mK. This value is slightly higher than the maximum magnitude of the dipolar interaction between the layers, $J_{dip} = 2.5$ mK, estimated using a simple approach [40].

To elucidate the exact role of the anisotropy and the interlayer interaction in the formation of the magnetic long-range order at T_λ it would be necessary to study the critical coefficients in the vicinity of the critical temperature, which was not possible from the measurements on the powdered sample due to the rounding effects at the λ-like anomaly. In the case of an isotropic 2D HAF a non-monotonous field dependence of the critical temperature is expected with a field-induced easy-plane behavior [41,42]. A more complex phase diagram is obtained when an easy-axis anisotropy is present with an Ising-type 2D ordering in the low-field region followed by a field-induced *XY*-like phase at higher magnetic fields [43–45]. To carry out such measurements in a wide range of magnetic fields and at very low temperatures is rather difficult and time consuming and is planned in the future.

4. Conclusions

By a relatively facile way a new compound, $[Cu(bmen)_2][Pt(CN)_4]$ (**1**), was prepared. The presence of individual functional groups and the composition of **1** were proved by infrared spectroscopy and CHN analysis. The study of thermal properties of **1** showed a three-step decomposition consisting of liberation of two *bmen* molecules and three cyano groups from one formula unit. The UV–VIS spectrum of **1** indicates the presence of six-coordinated Cu(II) atoms in the form of deformed octahedrons what was definitely confirmed by an X-ray analysis. The structure is formed by infinite zigzag covalent chains, parallel to the *a* axis, which are bound into sheets, lying in *ab* plane, by relatively weak hydrogen bonds of N–H···N type.

The analysis of the magnetic properties of **1** suggests that although having a chain-like crystal structure, the title compound exhibits a 2D magnetic structure with exchange coupling $J/k_B = -0.6$ K, including the influence of very weak interlayer exchange coupling. The 2D magnetic structure can be explained by the fact that the magnetic $d_{x^2-y^2}$ orbital is oriented within the equatorial plane of the local octahedron due to the Jahn-Teller distortion and is not involved in the covalent bonds. Consequently, the exchange path between the Cu(II) atoms is preferred through hydrogen bonds creating a square network and not through the covalent bonds within the chains.

Supplementary material

CCDC 692343 contains the supplementary crystallographic data for this paper. These data can be obtained free of charge via www.ccdc.cam.ac.uk/conts/retrieving.html (or from the CCDC, 12 Union Road, Cambridge CB2 1EZ, UK; fax: +44 1223 336033; e-mail: deposit@ccdc.cam.ac.uk).

Acknowledgments

This work was supported by the Grants of the Slovak Grant Agency VEGA nos. 1/0079/08 and 1/3027/06, by the Research and Development Support Agency APVV nos. 0006-07 and 0058-07. Part of this work was supported by the DFG. One of the authors (M.V.) thanks DAAD for financial support and hospitality of Martin-Luther-University. The financial support of US Steel—DZ Energetika Košice is acknowledged.

Appendix A. Supplementary material

Supplementary data associated with this article can be found in the online version at doi:10.1016/j.jssc.2008.10.017.

References

[1] M. Pilkington, S. Decurtins, in: A. McCleverty, T.J. Meyer (Eds.), Comprehensive Coordination Chemistry II, Vol. 7, Elsevier, Amsterdam, 2004.
[2] J. Černák, M. Orendáč, I. Potočňák, J. Chomič, A. Orendáčová, J. Skoršepa, A. Feher, Coord. Chem. Rev. 224 (2002) 51.
[3] S. Tanase, J. Reedijg, Coord. Chem. Rev. 250 (2006) 2501.
[4] I. Muga, J.M. Gutierrez-Zorrilla, P. Vitoria, P. Roman, L. Lezama, J.I. Beitia, Eur. J. Inorg. Chem. (2004) 1886.
[5] I. Potočňák, M. Vavra, E. Čižmár, K. Tibenská, A. Orendáčová, D. Steinborn, Ch. Wagner, M. Dušek, K. Fejfarová, H. Schmidt, T. Műller, M. Orendáč, A. Feher, J. Solid State Chem. 179 (2006) 1965.
[6] J.P. Zhang, R.S. Wang, M. Baumgarten, Mol. Cryst. Liq. Cryst. 306 (1997) 119.
[7] R. Boča, Coord. Chem. Rev. 173 (1998) 167.
[8] M. Orendáč, A. Orendáčová, J. Černák, A. Feher, Solid State Commun. 94 (1995) 833.
[9] J. Černák, J. Skoršepa, K.A. Abboud, M.W. Meisel, M. Orendáč, A. Orendáčová, A. Feher, Inorg. Chim. Acta 326 (2001) 3.
[10] J. Kuchár, J. Černák, Z. Mayerová, P. Kubáček, Z. Žák, Solid State Phenom. 90 (2003) 328.
[11] J. Hanko, M. Orendáč, J. Kuchár, Z. Žák, J. Černák, A. Orendáčová, A. Feher, Solid State Commun. 142 (2007) 128.
[12] N. Mermin, H. Wagner, Phys. Rev. Lett. 17 (1966) 1133.
[13] A. Cuccoli, T. Roscilde, V. Tognetti, R. Vaia, P. Verrucchi, Phys. Rev. B 67 (2003) 104414.
[14] V.L. Berezinskii, Zh. Eksp. Teor. Fiz. 59 (1970) 907.
[15] V.L. Berezinskii, Zh. Eksp. Teor. Fiz. 61 (1971) 1144.

[16] J.M. Kosterlitz, D.J. Thouless, J. Phys. C 5 (1972) L124.
[17] J.M. Kosterlitz, D.J. Thouless, J. Phys. C 6 (1973) 1181.
[18] G.B. Kaufmann, Inorg. Synth. 9 (1967) 182.
[19] S. Riegel, G. Webber, J. Phys. E 19 (1986) 790.
[20] Oxford Diffraction, Crysalis CCD and Crysalis RED, Oxford Diffraction Ltd., Oxford, UK, 2004.
[21] G.M. Sheldrick, SHELXS97 and SHELXL97, University of Gőttingen, Gőttingen, Germany, 1997.
[22] M. Nardelli, J. Appl. Crystallogr. 28 (1995) 659.
[23] K. Brandenburg, DIAMOND (Release 2.1e) Crystal Impact GbR, Bonn, Germany, 2000.
[24] Z. Gabelica, Spectrochim. Acta 32A (2) (1976) 337.
[25] K. Nakamoto, Infrared and Raman Spectra of Inorganic and Coordination Compounds, Part B: Applications in Coordination, Organometallic, and Bioinorganic Chemistry, Wiley, New York, 1997.
[26] A.M. Golub, H. Köhler, V.V. Skopenko, Chemistry of Pseudohalides, Elsevier, Amsterdam, 1986.
[27] C.A. Bignozzi, C. Chiorboli, M.T. Indelli, F. Scandola, V. Bertolasi, G. Gilli, J. Chem. Soc. Dalton Trans. (1994) 2391.
[28] J.A. Abys, G. Ogar, W.M. Risen Jr., Inorg. Chem. 20 (1981) 4446.
[29] J. Kuchár, J. Černák, K.A. Abboud, Acta Cryst. C 60 (2004) 492.
[30] M.L. Flay, H. Vahrenkamp, Eur. J. Inorg. Chem. (2003) 1719.
[31] S. Stoll, A. Schweiger, J. Magn. Reson. 178 (2006) 42.
[32] D. Gatteschi, A. Bencini, Electron Paramagnetic Resonance of Exchange Coupled Systems, Springer, Berlin, 1990.
[33] O. Kahn, Molecular Magnetism, Wiley, New York, 1985.
[34] L.J. de Jongh, A.R. Miedema, Adv. Phys. 23 (1974) 1.
[35] M.S. Makivic, H.-Q. Ding, Phys. Rev. B 43 (1991) 3562.
[36] B. Bernu, G. Misguich, Phys. Rev. B 63 (2001) 134409.
[37] P. Sengupta, A.W. Sandvik, R.R.P. Singh, Phys. Rev. B 68 (2003) 094423.
[38] R.D. Willet, Magneto-Structural Correlations in Exchange Coupled Systems, Riedel Publishing Company, 1985.
[39] C. Yasudo, S. Todo, K. Hukushima, F. Alet, M. Keller, M. Troyer, H. Takayama, Phys. Rev. Lett. 94 (2005) 217201.
[40] C.M. Wynn, M.A. Girtu, W.B. Brinckerhoff, K.-I. Sugiura, J.S. Miller, A.J. Epstein, Chem. Mater. 9 (1997) 2156.
[41] A.S.T. Pires, Phys. Rev. B 50 (1994) 9592.
[42] A. Cuccoli, T. Roscilde, R. Vaia, P. Verrucchi, Phys. Rev. B 68 (2003) 060402(R).
[43] A. Pelissetto, E. Vicari, Phys. Rev. B 76 (2007) 024436.
[44] R. van de Kamp, M. Steiner, H. Tietze-Jaensch, Physica B 241–243 (1998) 570.
[45] B.V. Costa, A.S.T. Pires, J. Magn. Magn. Mater. 262 (2003) 316.